Research Article | Vol. 15, No. 1 / 1 Jan 2024 / Biomedical Optics Express 294
Biomedical Optics EXPRESS

High-Q Fano resonances in all-dielectric metastructures for enhanced optical biosensing applications

HUAWEI CHEN,[1] XINYE FAN,[1,2,3,4,6] WENJING FANG,[1,3,4,7] BINGYUAN ZHANG,[1,3] SHUANGSHUANG CAO,[1] QINGHE SUN,[1] DANDAN WANG,[1] HUIJUAN NIU,[1,3,4] CHUANCHUAN LI,[2] XIN WEI,[2] CHENGLIN BAI,[1,3,4] AND SANTOSH KUMAR[1,3,5,8]

[1]*School of Physics Science and Information Engineering, Liaocheng University, Liaocheng 252000, China*
[2]*Institute of Semiconductors, Chinese Academy of Sciences, Beijing 100083, China*
[3]*Shandong Provincial Key Laboratory of Optical Communication Science and Technology, Liaocheng 252000, China*
[4]*Liaocheng Key Laboratory of Industrial-Internet Research and Application, Liaocheng 252000, China*
[5]*Department of Electronics and Communication Engineering, KL Deemed to be University, Guntur, Andhra Pradesh 522302, India*
[6]*fanxinye@yeah.net*
[7]*fwj0929@163.com*
[8]*santosh@lcu.edu.cn*

Abstract: Fano resonance with high Q-factor is considered to play an important role in the field of refractive index sensing. In this paper, we theoretically and experimentally investigate a refractive index sensor with high performance, realizing a new approach to excite multiple Fano resonances of high Q-factor by introducing an asymmetric parameter to generate a quasi-bound state in the continuum (BIC). Combined with the electromagnetic properties, the formation mechanism of Fano resonances in multiple different excitation modes is analyzed and the resonant modes of the three resonant peaks are analyzed as toroidal dipole (TD), magnetic quadrupole (MQ), and magnetic dipole (MD), respectively. The simulation results show that the proposed metastructure has excellent sensing properties with a Q-factor of 3668, sensitivity of 350 nm/RIU, and figure of merit (FOM) of 1000. Furthermore, the metastructure has been fabricated and investigated experimentally, and the result shows that its maximum Q-factor, sensitivity and FOM can reach 634, 233 nm/RIU and 115, respectively. The proposed metastructure is believed to further contribute to the development of biosensors, nonlinear optics, and lasers.

1. Introduction

Resonance with high Q-factor is considered to improve the performance of devices, including ultra-high sensitivity sensors [1–3], optical switches [4,5], semiconductor lasers [6,7], and nonlinear optics [8–10]. It is a great way to achieve high Q-factor by adopting Fano resonance, which is a scattering resonance phenomenon capable of producing asymmetric linearity [11–13].

Fano resonance is generally excited by the effect of destructive interference between the broad bright mode and the narrow dark mode [14,15]. All-dielectric nanoparticles become an effective way to obtain high Q-factor Fano resonance because of low radiation loss [16,17]. Fano resonance generated by all-dielectric metastructure evolves from a single resonance to multiple resonances [18,19]. Multiple Fano resonances offer great advantages in multi-wavelength surface-enhanced spectroscopy and multi-channel sensors [20]. An all-dielectric metastructure with two semicircularly controlled silicon rectangles etched inside the cell was designed by Yu *et al.*, which excited three Fano resonance peaks and the Q-factor can reach 2617 [21].

#510149 https://doi.org/10.1364/BOE.510149
Journal © 2024 Received 24 Oct 2023; revised 11 Dec 2023; accepted 11 Dec 2023; published 18 Dec 2023

Biomedical Optics EXPRESS

Wang *et al.* proposed a periodic all-dielectric nanodisk dimer, two Fano resonance peaks were excited with a maximum Q-factor of 2750 [22]. In addition, all-dielectric metastructure has the advantages, including device fabrication cost and complementary metal oxide semiconductor (CMOS) process compatibility issues [23].

An efficient method for high Q-factor Fano resonance to be achieved in an all-dielectric metastructure is the bound state in the continuum (BIC) [24,25]. Owing to the spatial asymmetry of the modes and spatially symmetric incompatibility of external radiated waves, the ideal BIC is characterized by a terrifically high Q-factor and an extremely narrow linewidth [26–28]. The ideal BIC not observed in practical applications is transformed to a quasi-BIC mode when the symmetry of the all-dielectric metastructure is broken [29]. The quasi-BIC mode is responsible for the new Fano resonance peaks generated by the asymmetric structure, which can be observed in the transmission spectrum [30].

The excitation of Fano resonance implies the occurrence of electromagnetic wave scattering phenomena [31,32]. As an important contribution to the scattering field, toroidal dipole (TD) radiation is often masked by electric dipole (ED) and magnetic dipole (MD) in resonances excited in metallic metasurfaces, which cannot be dominated [33,34]. Compared to plasma nanostructures, the excited TD can be better facilitated by the interaction between light and matter in all-dielectric metastructure, utilizing weak free-space coupling to achieve high Q-factor Fano resonances [35].

In this paper, an all-dielectric metastructure is designed and fabricated, which can generate multiple Fano resonances. The metastructure consisting of a crossed rod and four fan-shaped silicon blocks is placed periodically on a substrate that is silicon dioxide (SiO_2). The symmetry of the metastructure is broken by changing the radius of two of the fan-shaped silicon blocks, three Fano resonances with high Q-factors are generated. The Q-factor of the excited Fano resonance can reach up to 3668, the sensitivity of the maximum can get up to 350 nm/RIU, and the figure of merit (FOM) with a maximum of 1000 RIU^{-1}. In addition, experiments are conducted on the proposed structure, and the results show that the maximum sensitivity is 233 nm/RIU. It is shown that the metastructure has promising applications in the field of refractive index sensors and optical switches.

2. Model

A single period cell of the designed structure is shown in Fig. 1(a). A crossed rod and four fan-shaped silicon blocks are placed on the substrate that is SiO_2. The labeled P_x and P_y in Fig. 1(a) are the periods in the x and y directions, respectively. The length of P_x and P_y is 800 nm, and the silicon block height (h) is 200 nm. The crossed rod silicon block has a length (L_1) of 700 nm and a width (L_2) of 100 nm, which is placed in the center of the substrate. The four fan-shaped silicon are distributed around the crossed rod silicon block, the radii of f_1 and f_2 (r_1) are 185 nm, and the radii of f_3 and f_4 (r_2) are 200 nm. The distance (g) of the fan-shaped silicon block to the crossed rod silicon block is 100 nm. The ideal BIC is converted to quasi-BIC because of $r_1 \neq r_2$. The asymmetric degree of metastructure is described by defining the asymmetric parameter $\delta = r_2 - r_1$. The method for simulating the values is the finite difference in time-domain (FDTD). The x and y directions are set as periodic boundary conditions, and the z direction is set differently as a perfect matching layer (PML). The incident wave will decay rapidly under the effect of loss at the time of entering the PML layer. A Light source illuminates the designed structure that is a y-polarized plane wave perpendicular to the z-axis. The refractive index of Si and SiO_2 used in the simulations are all taken from the Palik refractive index library [36]. The transmission spectra and the electromagnetic field distribution of the proposed metastructure are mainly analyzed.

Biomedical Optics EXPRESS

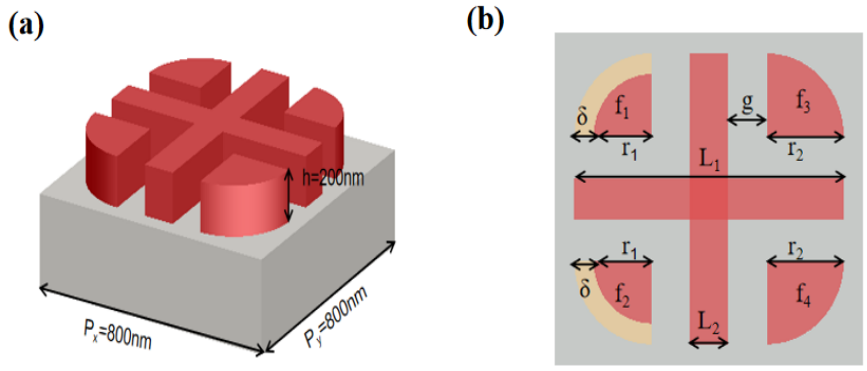

Fig. 1. (a) Schematic diagram of a single cycle of the designed metastructure, consisting of a cross rod and four sector-shaped silicon blocks placed on a silica substrate. (b) Top view of the metastructure and its corresponding geometric parameters.

3. Simulation results and discussion

In the simulation, the metastructure is placed in a liquid medium with a refractive index of 1.43. The metastructure is symmetric while $\delta = 0$, the obtained simulated transmission spectrum is shown as the black line in Fig. 2(a). There is only one peak at 1299 nm in the transmission spectrum at this time. The structure symmetry is broken while $\delta = 15$ nm and a zero-level radiation channel is created, leading to the BIC conversion to the quasi-BIC mode. The red line in Fig. 2(b) illustrates the transmission spectrum obtained from the simulation. The original resonance peak is slightly blue-shifted to 1295 nm. Two new Fano resonance peaks are excited at 1283 nm and 1327 nm for the asymmetric structure compared to the symmetric structure, respectively.

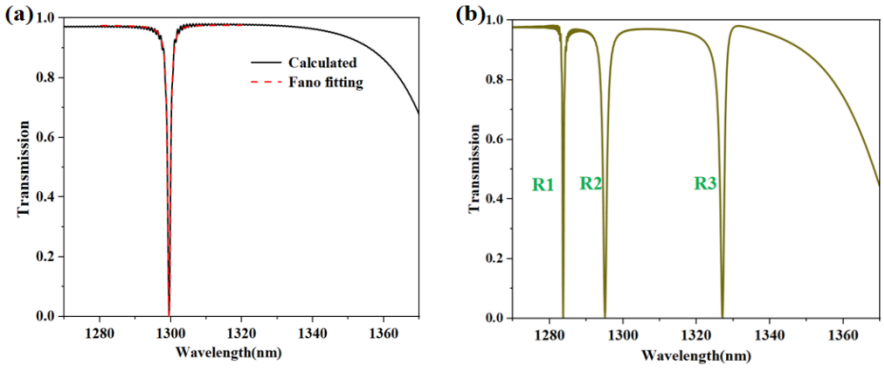

Fig. 2. Transmission spectrum of the designed metastructure. (a) Transmission spectra and fitted curves of the designed infrastructure at symmetry. (b) Transmission spectrum of the designed metastructure while $\delta = 15$ nm.

Analysis of the two peaks of quasi-BIC excitation can be performed using the following Fano formula:

$$T = \left| a_1 + ia_2 + \frac{b}{\omega - \omega_0 + i\gamma} \right|^2 \tag{1}$$

in which, a_1, a_2 and b are constant real numbers, ω_0 is the resonant frequency, and γ is the damping loss. The Fano spectral features of the proposed metastructure can be accurately

Biomedical Optics EXPRESS

reproduced by the above equation, and the red line segment in Fig. 2(a) shows the fitted Fano linearity. In addition, the above equation can be used to extract the Q-factor of the Fano resonance, which is calculated as

$$Q = \frac{\omega_0}{2\gamma} \tag{2}$$

The Q-factor of the resonance peak can reach 3668 ($\omega_0 = 0.968$ eV and $\gamma = 0.1319\times10^{-3}$ eV), 1080 ($\omega_0 = 0.959$ eV and $\gamma = 0.4439\times10^{-3}$ eV), 1045 ($\omega_0 = 0.936$ eV and $\gamma = 0.4478\times10^{-3}$ eV) after calculation while $\delta = 15$ nm.

In addition, the relationship between the Q-factor and the asymmetry parameter is further investigated. The radiation channel between the non-radiative bound state and the free space continuum is constructed when the symmetry of the structure receives broken, allowing the BIC mode to radiate outward under the excitation of y-polarization, which excites the Fano resonance with high Q-factor. $\alpha = \Delta S/S$ is introduced as an asymmetric parameter, in which ΔS is the area that decreases with decreasing radius and S is the total area of the silicon block, Fig. 3(b) can represent ΔS and S. more clearly. The Q-factor of the excited Fano resonance is related to the asymmetry parameter α as $Q \propto \alpha^{-2}$ [37], as shown in Fig. 3(a).

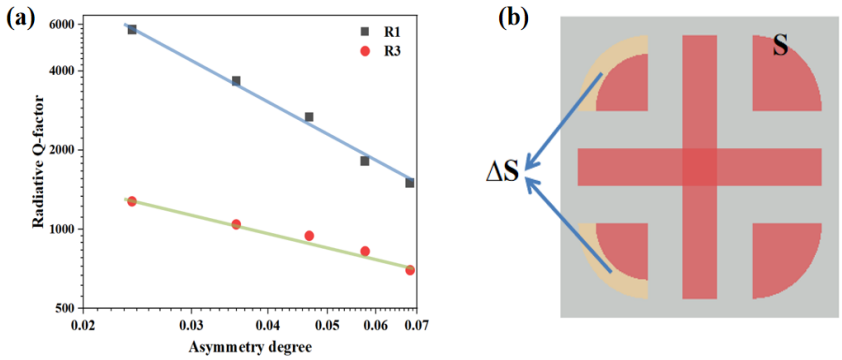

Fig. 3. (a) Correspondence plots of different asymmetry parameters with Q-factors. (b) Schematic representation of ΔS and S.

To better analyze the Fano resonance peaks and explain the physical mechanism of multiple resonance peaks, the optical field at the resonance peaks is simulated. Table 1 shows the electromagnetic field distribution of the cross-section at the three resonance peaks. The resonant mode of R1 can be obtained from the analysis on the graph as a typical TD resonance. Two magnetic field loops in opposite directions can be observed in the $x-y$ ane of R1, meaning that the electric field is opposite in the direction along the loop surface. The electric field in the $y-z$ plane of R1 forms two arrows in opposite directions, which can form a complete ring, so there is a TD resonance in the x-direction. The $x-y$ plane diagram of R2 shows the electric field distribution, and the four magnetic loop currents generated will produce four typical MD resonances. Based on the magnetic field distribution in the $x-z$ plane and $y-z$ plane of R2, it can be inferred that the two adjacent magnetic loop currents in the $x-y$ plane can be combined to form a TD resonant mode. The formed TD resonance modes are observed in the diagonal direction of the metastructure, the two TD modes on the same diagonal have opposite moment directions. It presents that the resonant mode is magnetic quadrupole (MQ) resonance. A current loop can be observed in the $x-y$ plane diagram of R3 and a magnetic field is formed in the $y-z$ plane in the negative direction along the z-axis, resulting in an MD resonance in the z-direction.

In order to investigate the effect of the relevant parameters on the metastructure transmission spectrum, simulations are performed for the variation of different geometric parameters for the case of $\delta = 15$ nm, as shown in Fig. 4. Figure 4(a) shows the transmission spectrum curve of the

Biomedical Optics EXPRESS

Table 1. The electromagnetic field distribution of the asymmetric metastructure while δ = 15 nm.

Fano Resonance Peak	R1(1283nm)	R2(1295nm)	R3(1327nm)
Diagram of electric field	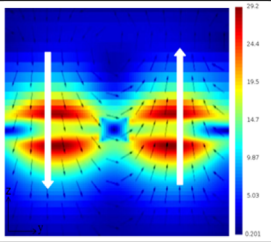	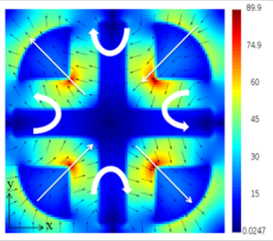	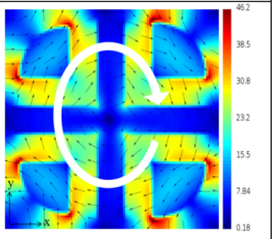
Diagram of magnetic field	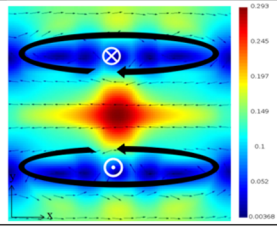	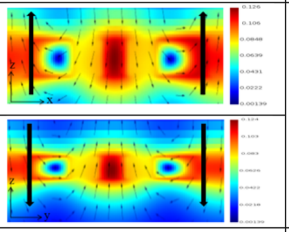	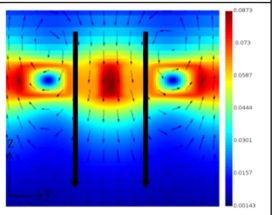
Resonance mode	TD	MQ	MD

metastructure when the length (L_1) of the crossed rod silicon block is varied from 650 nm to 750 nm. It can be seen that the three resonance peaks are not sensitive to L_1, especially since the position of R3 hardly changes, and R1 and R2 are only slightly red-shifted. All resonance peaks are very sensitive to the height h of the silicon block, and as h increases from 195 nm to 205 nm, the resonance peaks are severely red-shifted. Based on Fig. 4(b), this conclusion can be easily drawn. With the increasing distance from the fan-shaped silicon block to the crossed rod silicon block, the other two resonance peaks hardly change except for a slight red shift of R1. The resonance peaks are not sensitive to the interval (g) shown in Fig. 4(c). The transmission spectrum of the metastructure at different periods (P) is shown in Fig. 4(d). The metastructure is sensitive to P, which not only shows a red shift in the resonance peak but also a large change in the linewidth of R1 and R2.

Analyzing the above, it can be seen that the proposed metastructure is tunable and the transmission spectrum can change with the geometric parameters. In addition, the effect of the polarization direction of the light source on the transmission spectrum is also investigated for additional applications.

The transmission spectra when the metastructure is irradiated by different polarization directions are shown in Fig. 5(b). With different polarization directions of irradiation, the resulting Fano resonance peaks are reflected in Fig. 5(a) as highlighted in the shaded area. The resonance peaks are labeled as mode I, II, III and IV, respectively. As the increasing polarization angle θ, the transmittance of mode I gradually decrease, and mode II remains unchanged. In addition, the transmittance of mode III and mode IV gradually increases, and all the modes are not shifted. It is clear that means that modes I, III and IV have polarization dependence and great potential for optical switching applications.

In order to thoroughly investigate the effect of the extinction coefficient (k) of the measured liquid on the transmission spectrum, the symmetric and asymmetric transmission spectra are simulated for different extinction coefficients, and the results are shown in Fig. 6. The linewidth of the Fano resonance peak increases and the modulation depth decreases as k increasing, which induces a decrease in the Q-factor. A larger extinction coefficient (k) means that the liquid absorbs and scatters light more severely, leading to a gradual disappearance of the Fano resonance.

Biomedical Optics EXPRESS

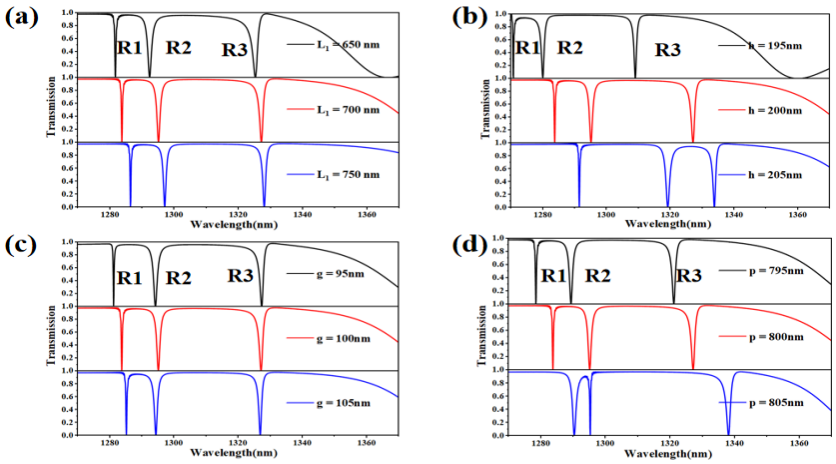

Fig. 4. Transmission spectrum for tuning the different geometrical parameters of the metastructure. (a) Length of crossed rod silicon block(L_1), (b) Height of silicon block(h), (c) Distance from fan-shaped silicon block to crossed rod silicon block(g), (d) Cycles of metastructure (P).

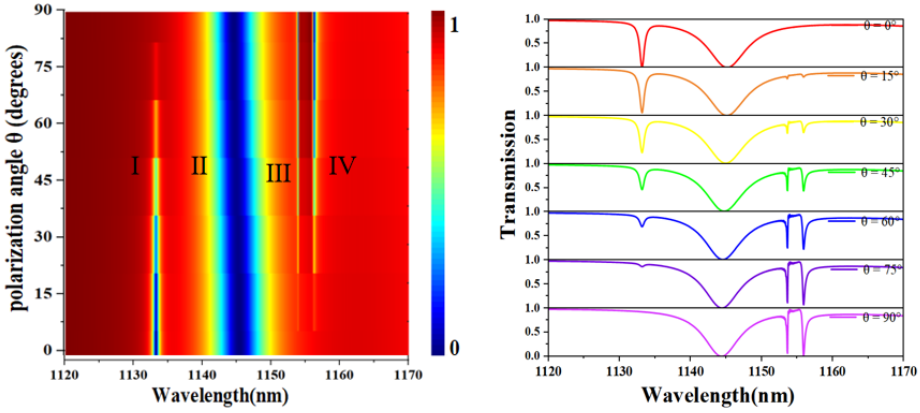

Fig. 5. Transmission spectra at different polarization angles for δ = 15 nm.

Biomedical Optics EXPRESS

Compared to R2, R1 and R3 are more sensitive to k, suggesting that the same k produces different effects for different modes of Fano resonance.

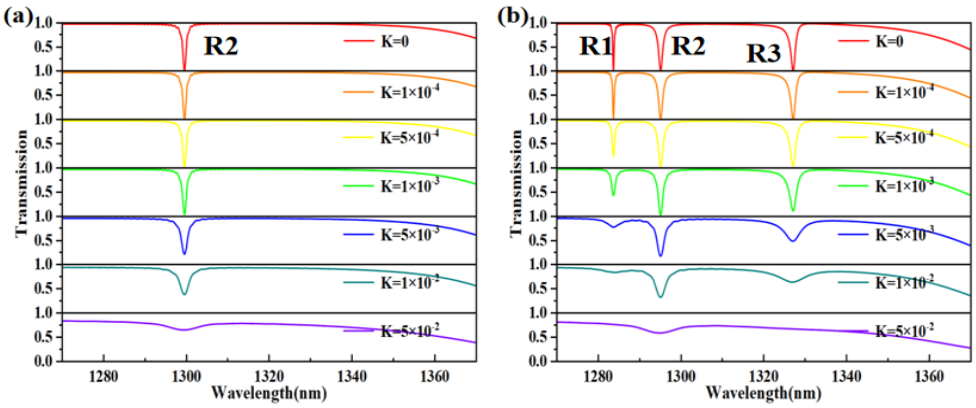

Fig. 6. (a) Transmission spectra of symmetric structures with different extinction coefficients, (b)Transmission spectra of asymmetric structures with different extinction coefficients.

The proposed metastructure is suitable for refractive index sensors because of its ability to produce Fano resonance peaks with high Q-factor and low radiation loss. The sensing characteristics of the metastructure are studied by defining the refractive index RI of the liquid covering the outside of the structure as n. Simulations are performed when n is taken from 1.41 to 1.45, and the results are shown in Fig. 7. Figure 7(a) shows the transmission spectra of R1 and R2 at different refractive indexes, and Fig. 7(b) shows the transmission spectrum of R3.

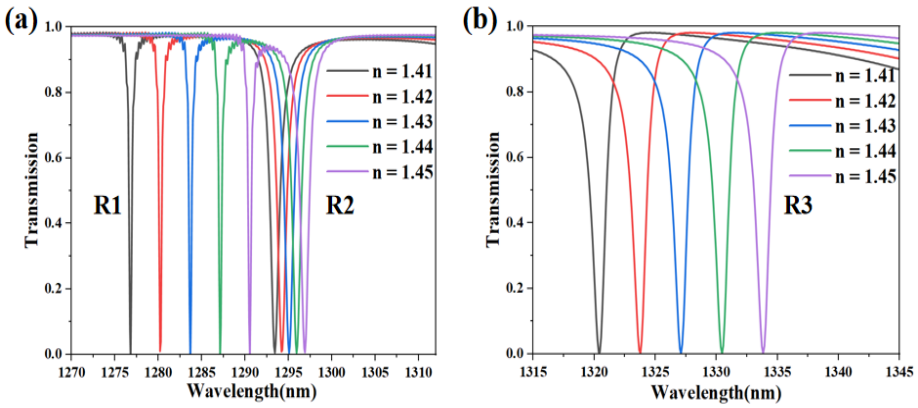

Fig. 7. Transmission spectra at different refractive indexes. (a) Transmission spectra of two peaks of R1 and R2 at different refractive indexes. (b) Transmission spectra of R3 at different refractive indexes.

As n increases from 1.41 to 1.45, the resonance peaks are red-shifted. R1 and R3 are significantly red-shifted, while R2 is only slightly red-shifted. In addition to Q, the other two metrics that can reflect the meta-structure sensing performance are sensitivity (S) and FOM. The sensitivity is the ratio of the offset of the resonance peak to the refractive index difference, and the equation is [38]:

$$S = \frac{\Delta\lambda(nm)}{\Delta n(RIU)} \tag{3}$$

Biomedical Optics EXPRESS

The sensitivities of the three resonance peaks were calculated as 350 nm/RIU, 97 nm/RIU and 346 nm/RIU, respectively, according to Eq. (3).

FOM is the ratio of sensitivity to the full width at half peak (FWHM) [39], Eq. (4):

$$FOM = \frac{S(nm/RIU)}{FWHM(nm)} \tag{4}$$

The FOM of the three resonance peaks are calculated to be 1000, 81, and 273, respectively.

In addition, the sensitivity and FOM of the proposed meta-structure are compared with the literature and the results are shown in Table 2. It can be seen that compared to earlier sensors, the metastructure in this paper is more suitable for sensing devices because has higher sensitivity and FOM.

Table 2. Sensitivity and FOM of comparison with other existing sensors.

Sensor Type	S (nm/RIU)	FOM(RIU^{-1})	Ref.
Double square hollow	287.5	389	[40]
Semicircular holes	300	440	[21]
U-shaped silicon cylinder	203	29	[41]
Metastructure consists of two semicircular nanopores and a narrow connecting channel	265	883	[42]
Broken-symmetry dimer-type metasurface	305	68	[43]
Asymmetric all-dielectric nanoarrays	350	1000	This work

4. Experimental results and discussion

The material used to fabricate the proposed metastructure is a silicon-on-insulator substrate with 200 nm silicon on top. The main geometric parameters are: $P_x = P_y = 800$ nm, $h = 200$ nm, $L_1 = 700$ nm, $L_2 = 100$ nm, $r_1 = 185$ nm, $r_2 = 200$ nm, $g = 100$ nm. The preparation process of the metastructure is shown in Fig. 8. The device preparation procedure consists of the following steps: cleaning of the SOI substrate, low-pressure chemical vapor deposition (LPCVD), spin coating of the resist, electron beam lithography (EBL), development, inductively coupled plasma (ICP) etching and removal of the resist. The preparation process is simple and the actual structure applied to the sensor can be obtained at low cost. An SOI sample of 800 μm * 800 μm with one million nanoparticle array units is obtained after preparation and its SEM image is shown in Fig. 9. From the SEM image, the homogeneity and smoothness of the sample are excellent.

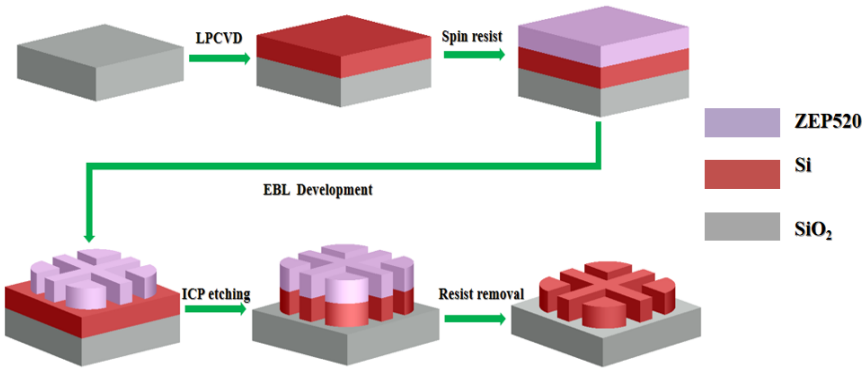

Fig. 8. The fabrication process flow chart of the metastructure.

Biomedical Optics EXPRESS

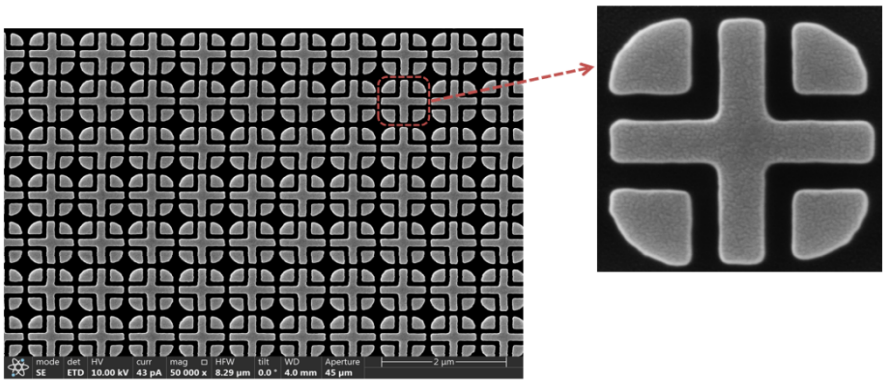

Fig. 9. SEM picture of the developed sample.

A sensing test system is set up to test the sensing performance of the samples, the sketch of which is shown in Fig. 10. The system is composed of a light source, a pair of fiber optic collimators and a spectrometer. The light source is a broad-spectrum laser (470 nm-2400 nm). The light beam output from the light source is collimated by a fiber collimator, and then irradiated to the samples which are immersed in different refractive indexes, and the beam after pasing through the samples is collected by another fiber collimator, and its transmission spectrum is reflected to the spectrometer.

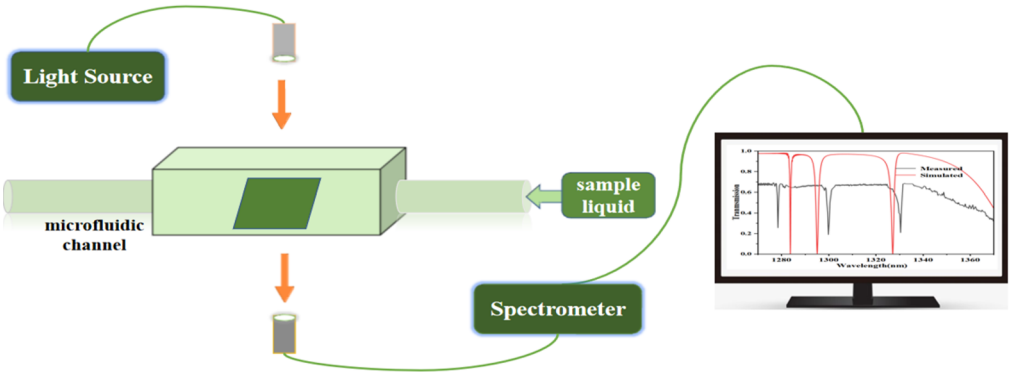

Fig. 10. Systems for testing metastructure sensing performance.

The measured refractive index of the liquid is changed by varying the sucrose concentration. Multiple measurements of sucrose solutions with concentrations of 45%, 50%, 55%, 60%, and 65% using an Abbe refractometer yielded refractive indexes of 1.4075, 1.4157, 1.4238, 1.4302, and 1.4402, respectively. Figure 11(a) shows a comparison of the test transmission spectrum with the simulated transmission spectrum. The modulation depths and Q-factors of the transmission spectra obtained from the tests are lower compared to the simulation results, which is due to errors in the measurement process or dimensional errors in the sample preparation. The solubility of the liquid to be tested is continuously varied and the transmission spectra of the test at different refractive indexes are obtained. Figure 11 (b) shows the transmission spectra tested at different refractive indexes. The maximum sensitivity of the sample is calculated to be 233 nm/RIU.

In this case, errors are generated during the structure preparation process, which introduces scattering losses, thus, affecting the coherence of the sensor. The extra losses in Si are caused by the creation of surface states in the reactive ion etching process, which results in a slight increase

Biomedical Optics EXPRESS

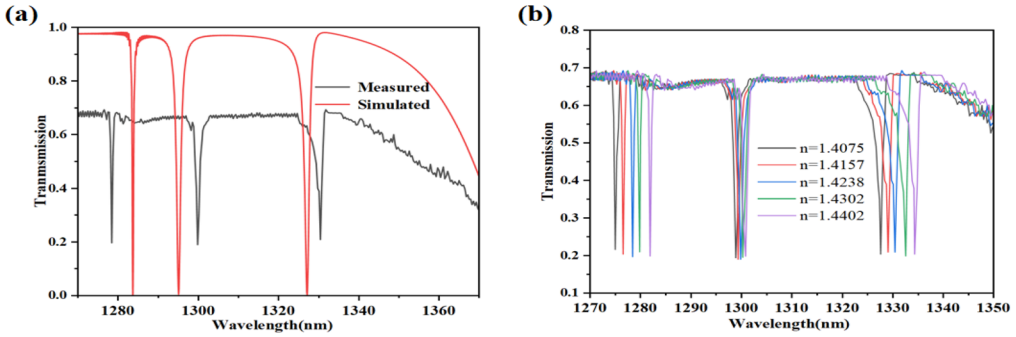

Fig. 11. (a) Testing and Simulation of Transmission Spectra, (b) Test transmission spectra at different refractive indexes.

of uptake compared to the theory in the array. In addition, the environmental parameters in the experiment cannot be kept constant and cannot be identical to the simulated environment. As a result, there is a deviation between the experimental and simulation results, and the modulation depth becomes smaller, but this is acceptable.

The results of the experiments are compared with those of other types of sensors in Table 3. The results show that the proposed device has high performance parameters.

Table 3. Performance comparison of the proposed sensor with other existing sensors.

Sensor Type	Q-factor	S (nm/RIU)	FOM(RIU^{-1})	Ref.
Single-layer guided mode resonance structure	n.r.[a]	229.43	31.52	[44]
Hollow cuboids	728	161	n.r.[a]	[45]
Silicon rods and rings	483	289	103	[46]
Two defective columns	94	337	29	[47]
Asymmetric all-dielectric nanoarrays	634	233	115	This work

[a]not reported

5. Conclusions

In summary, a metastructure that can generate multiple Fano resonance peaks is proposed in this paper. The resonance modes of each resonance peak, TD, MQ and MD, are obtained by analyzing the electromagnetic field. The Q-factors of all three Fano resonance peaks are superior, with the highest and lowest being 3668 and 1045, respectively. As a result of the simulation, it is found that the generated resonance peak is sensitive to refractive index, the maximum sensitivity obtained is at 350 nm/RIU, and the maximum FOM is 1000. Experimental tests show that the proposed metastructure has excellent sensing characteristics. In addition, the position of the resonance peaks can be flexibly adjusted by modulating the geometric parameters of the metastructure, making the metastructure great potential for the application of optical refractive index sensors.

Funding. Liaocheng University (318052341); The Cultivation Plan for Young Scholars in Universities of Shandong Province (2021RC085); The Natural Foundation of Shandong Province (ZR2021MF053, ZR2021MF070, ZR2022MF253, ZR2022MF305); The Open Fund of the Key State Laboratory (BUPT, IPOC) (IPOC2019A009, IPOC2021B07); Double-Hundred Talent Plan of Shandong Province.

Disclosures. The authors declare no conflicts of interest.

Data availability. Data underlying the results presented in this paper are not publicly available at this time but may be obtained from the authors upon reasonable request.

Biomedical Optics EXPRESS

References

1. M. Gupta, Y. K. Srivastava, M. Manjappa, *et al.*, "Sensing with toroidal metamaterial," Appl. Phys. Lett. **110**(12), 121108 (2017).
2. A. A. Siraji and Y. Zhao, "High-sensitivity and high-Q-factor glass photonic crystal cavity and its applications as sensors," Opt. Lett. **40**(7), 1508–1511 (2015).
3. J. Yu, J. Zhu, S. Ye, *et al.*, "Ultra-wide sensing range plasmonic refractive index sensor based on a two-dimensional circular-hole grating engraved on a gold film," Results Phys. **26**, 104396 (2021).
4. Z. Han and J. Yang, "All-optical self-switching with ultralow incident laser intensity assisted by Bound state in the continuum," Opt. Lett. **46**(3), 524–527 (2021).
5. M. Gupta, Y. K. Srivastava, and R. Singh, "A toroidal metamaterial switch," Adv. Mater. **30**(4), 1704845 (2018).
6. A. Kodigala, T. Lepetit, Q. Gu, *et al.*, "Lasing action from photonic bound states in continuum," Nature **541**(7636), 196–199 (2017).
7. M. Chinnasamy and K. Balasubramanian, "Investigation on laser induced fano resonance of hydrothermally synthesized Ag doped ZnO hierarchical nanoporous structure and its UV photodetector properties," Opt. Mater. **133**, 112873 (2022).
8. J. Butet and O. J. F. Martin, "Fano resonances in the nonlinear optical response of coupled plasmonic nanostructures," Opt. Express **22**(24), 29693 (2014).
9. S. Xiao, M. Qin, J. Duan, *et al.*, "Robust enhancement of high-harmonic generation from all-dielectric metasurfaces enabled by polarization-insensitive bound states in the continuum," Opt. Express **30**(18), 32590–35299 (2022).
10. S. Liu, E. S. P. Leong, G. Li, *et al.*, "Polarization-independent multiple Fano resonances in plasmonic nonamers for multimode-matching enhanced multiband second-harmonic generation," ACS Nano **10**(1), 1442–1453 (2016).
11. Y. Moritake, Y. Kanamori, and K. Hane, "Enhanced quality factor of Fano resonance in optical metamaterials by manipulating configuration of unit cells," Appl. Phys. Lett. **107**(21), 211108 (2015).
12. K. S. Modi, J. Kaur, S. P. Singh, *et al.*, "Extremely high figure of merit in all-dielectric split asymmetric arc metasurface for refractive index sensing," Opt. Commun. **462**, 125327 (2020).
13. Y. Wang, S. Yu, Z. Gao, *et al.*, "Excitations of Multiple Fano Resonances Based on Permittivity-Asymmetric Dielectric Meta-Surfaces for Nano-Sensors," IEEE Photonics J. **14**(1), 4613107 (2022).
14. V. A. Fedotov, M. Rose, S. L. Prosvirnin, *et al.*, "Sharp trapped-mode resonances in planar metamaterials with a broken structural symmetry," Phys. Rev. Lett. **99**(14), 147401 (2007).
15. K. Wang, Y. Wang, X. Wang, *et al.*, "All-dielectric refractive index sensor based on multiple fano resonance with high sensitivity in the long-wave infrared region," Coatings **12**(7), 970 (2022).
16. L. Zhao, H. Liu, Z. He, *et al.*, "Design of multi-narrowband metamaterial perfect absorbers in near-infrared band based on resonators asymmetric method and modified resonators stacked method," Opt. Commun. **420**, 95–103 (2018).
17. Y. Zhang, W. Liu, Z. Li, *et al.*, "High-quality-factor multiple Fano resonances for refractive index sensing," Opt. Lett. **43**(8), 1842–1845 (2018).
18. S. Yu, Y. Wang, Z. Gao, *et al.*, "Dual-band polarization-insensitive toroidal dipole quasi-bound states in the continuum in a permittivity-asymmetric all-dielectric meta-surface," Opt. Express **30**(3), 4084–4095 (2022).
19. W. Wang, L. Zheng, and J. Qi, "High Q-factor multiple Fano resonances for high-sensitivity sensing in all-dielectric nanocylinder dimer metamaterials," Appl. Phys. Express **12**(7), 075002 (2019).
20. S. Campione, S. Liu, L. I. Basilio, *et al.*, "Broken symmetry dielectric resonators for high quality factor Fano metasurfaces," ACS Photonics **3**(12), 2362–2367 (2016).
21. S. Yu, H. Li, Y. Wang, *et al.*, "Multiple Fano resonance excitation of all-dielectric nanoholes cuboid arrays in near infrared region," Results Phys. **28**(28), 104569 (2021).
22. W. Wang, L. Zheng, Y. Liu, *et al.*, "High-quality-factor multiple Fano resonances in free-standing all-dielectric nanodisk dimers for applications," Optik **207**, 163815 (2020).
23. P. Genevet, F. Capasso, F. Aieta, *et al.*, "Recent advances in planar optics: from plasmonic to dielectric metasurfaces," Optica **4**(1), 139 (2017).
24. L. Yang, S. Yu, H. Li, *et al.*, "Multiple Fano resonances excitation on all-dielectric nanohole arrays metasurfaces," Opt. Express **29**(10), 14905–14916 (2021).
25. F. Kebin, V. S. IIya, and J. P. Willie, "Dynamic bound states in the continuum," Optica **6**(2), 169–173 (2019).
26. E. N. Bulgakov and A. F. Sadreev, "Bound states in the continuum in photonic waveguides inspired by defects," Phys. Rev. B **78**(7), 075105 (2008).
27. K. Koshelev, G. Favraud, A. Bogdanov, *et al.*, "Nonradiating photonics with resonant dielectric nanostructures," Nanophotonics **8**(5), 725–745 (2019).
28. Z. Sadrieva, K. Frizyuk, M. Petrov, *et al.*, "Multipolar origin of bound states in the continuum," Phys. Rev. B **100**(11), 115303 (2019).
29. L. Mao, P. Cheng, K. Liu, *et al.*, "Sieving nanometer enantiomers using bound states in the continuum from the metasurface," Nanoscale Adv. **4**(6), 1617–1625 (2022).
30. Q. Xu, X. Zhang, Q. Yang, *et al.*, "Polarization-controlled asymmetric excitation of surface plasmons," Optica **4**(9), 1044–1051 (2017).
31. Q. Xie, G. Dong, B. Wang, *et al.*, "High-Q Fano resonance in terahertz frequency based on an asymmetric metamaterial resonator," Nanoscale Res. Lett. **13**(1), 294 (2018).

Biomedical Optics EXPRESS

32. T. Lee, T. Nomura, X. Su, *et al.*, "Fano-like acoustic resonance for subwavelength directional sensing: 0-360 degree measurement," Adv. Sci. **7**(6), 1903101 (2020).
33. L. Cong, Y. K. Srivastava, and R. Singh, "Tailoring the multipoles in THz toroidal metamaterials," Appl. Phys. Lett. **111**(8), 081108 (2017).
34. A. E. Miroshnichenko, A. B. Evlyukhin, Y. F. Yu, *et al.*, "Nonradiating anapole modes in dielectric nanoparticles," Nat. Commun. **6**(1), 8069 (2015).
35. X. Luo, X. Li, T. Lang, *et al.*, "Excitation of high Q toroidal dipole resonance in an all-dielectric metasurface," Opt. Mater. Express **10**(2), 358–368 (2020).
36. A. Edwards, *Silicon (Si), Handbook of Optical Constants of Solids*, 2nd ed. (E. D. Palik, 1985).
37. K. Koshelev, S. Lepeshov, M. Liu, *et al.*, "Asymmetric metasurfaces with high-Q resonances governed by bound states in the continuum," Phys. Rev. Lett. **121**(19), 193903 (2018).
38. M. A. Abbas, A. Zubair, K. Riaz, *et al.*, "Engineering multimodal dielectric resonance of TiO_2 based nanostructures for high-performance refractive index sensing applications," Opt. Express **28**(16), 23509–23522 (2020).
39. G. D. Liu, X. Zhai, L. L. Wang, *et al.*, "A high-performance refractive index sensor based on Fano resonance in Si split-ring metasurface," Plasmonics **13**(1), 15–19 (2018).
40. H. Li, S. Yu, L. Yang, *et al.*, "High Q-factor multi-Fano resonances in all-dielectric double square hollow metamaterials," Opt. Laser Technol. **140**, 107072 (2021).
41. M. Qin, C. Pan, Y. Chen, *et al.*, "Electromagnetically induced transparency in all-dielectric U-shaped silicon metamaterials," Appl. Sci. **8**(10), 1799 (2018).
42. J. Xing, H. Li, S. Yu, *et al.*, "Multiple Fano resonances driven by bound states in the continuum in an all-dielectric nanoarrays system," AIP Adv. **13**(3), 035212 (2023).
43. Y. Jahani, E. R. Arvelo, F. Yesilkoy, *et al.*, "Imaging-based spectrometer-less optofluidic biosensors based on dielectric metasurfaces for detecting extracellular vesicles," Nat. Commun. **12**(1), 3246 (2021).
44. L. Qian, K. Wang, W. Zhu, *et al.*, "Enhanced sensing ability in a single-layer guided-mode resonant optical biosensor with deep grating," Opt. Commun. **452**, 273–280 (2019).
45. P. A. Jeong, M. D. Goldflam, S. Campione, *et al.*, "High quality factor toroidal resonances in dielectric metasurfaces," ACS Photonics **7**(7), 1699–1707 (2020).
46. Y. Yang, I. I. Kravchenko, D. P. Briggs, *et al.*, "All-dielectric metasurface analogue of electromagnetically induced transparency," Nat. Commun. **5**(1), 5753 (2014).
47. H. Zhao, X. Fan, X. Wei, *et al.*, "All-dielectric metastructure based on multiple Fano resonances with high sensitivity," Opt. Commun. **530**, 129193 (2023).